CHAPTER 1

MOTOR CURRENT SIGNATURE ANALYSIS FOR INDUCTION MOTORS

William T. Thomson

1.0 INTRODUCTION

In 1824, Francois Arago initially formulated the concept of a rotating magnetic field which was subsequently known as Arago's rotations. On June 28, 1879, Walter Bailey presented to the Royal Society of London, a paper entitled *A Mode of Producing Arago's Rotations,* in which he proposed an early form of the induction motor. On May 16, 1888, Nikola Tesla presented a paper on a "New System of Alternate Current Motors and Transformers" to The American Institute of Electrical Engineers [1.1]. This paper and Tesla's practical demonstrations proved how a rotating magnetic field could be produced and also verified its application to the principles of operation of an induction motor. Also, in April 1888, The Royal Academy of Sciences of Turin published Galileo Ferraris' research findings on his ac polyphase motor in which he presented the basis for the operation of an induction motor.

Nikola Tesla's contributions, which, very importantly, he patented in the United States in 1888 are considered to be the catalyst for the subsequent industrial development of the modern generation and distribution of electricity using the 3-phase alternating current (ac) system, which is universally used throughout the modern world. It is now generally accepted that Nikola Tesla's greatest achievement was his invention of the induction motor and these motors dwarf all other electric motors in industrial importance since they are used in their millions throughout industry around the world. Without this electrical machine, modern society as we know it today would probably not exist. The induction motor, without doubt is one of the greatest inventions of all time but one of which, it is sad to state, the world at large is completely unaware.

Induction motors typically consume 40–50% of the generated electricity in an industrialized country. In 2008, the United States was the largest consumer of electricity at 4,401,698 GWhrs/annum [1.2], hence the vast number of these motors used in industry becomes very clear. Induction motors are the "workhorses" of a modern industrialized country and as such, a condition assessment of their

Current Signature Analysis for Condition Monitoring of Cage Induction Motors: Industrial Application and Case Histories, First Edition. William T. Thomson and Ian Culbert.

operational integrity via condition monitoring is normal practice by end users to avoid the following:

(i) Unscheduled downtime and lost (delayed) production and income

(ii) Catastrophic failures

(iii) Hazardous operating conditions that may lead to major accidents

There are a number of key categories that cause failures in induction motors and these are

(i) Bearing failures

(ii) Stator winding failures

(iii) Broken rotor bars or end rings in cage induction motors

(iv) High airgap eccentricity and unbalanced magnetic pull that may lead to a consequential rotor to stator rub

Vibration monitoring and analysis to detect bearing faults in rotating plant (which includes induction motors) is well documented via thousands of published papers and also in text books and is therefore not the subject of this book. Stator winding failures and on-line partial discharge monitoring to assess the operational condition of high voltage (HV) stator windings are covered by Stone et al. [1.3].

This book is dedicated to motor current signature analysis (MCSA) for condition monitoring of 3-phase induction motors (SCIMs) and its content is specifically focused to suit the needs of industry. It differs from all other books on condition monitoring of electrical machines, for example, by Tavner et al. [1.4] which has a small part content (pp. 207–212) on current monitoring for rotor faults but does give a broad coverage of all the different condition monitoring technologies applicable in industry to electrical machines. A book by Toliyat et al. [1.5] provides a chapter on MCSA (Chapter 9, pp. 199–219), but there are no industrial case histories on this subject in that chapter and to quote the authors in the preface: "*the book was written to provide a full review of diagnostic technologies and as an application guide for graduate and undergraduate students.*" The book achieves its objectives and includes coverage on theoretical modeling, condition monitoring, and fault diagnosis for different types of electrical machines, but it is essentially a book for academia and students.

In contrast, this book is unique and the first of its kind since its central theme is on the industrial application of MCSA.

1. It contains a "unique data base" of 50 industrial case histories on the application of MCSA to 3-phase SCIMs in the range from 127 kW (170 HP) up to 10,160 kW (13,620 HP) at voltages from 415 V up to 13,800 V, and covers the following:

   (i) Successful and unsuccessful diagnosis of broken rotor bars in cage rotors.

   (ii) Successful diagnosis of unacceptable levels of airgap eccentricity in cage induction motors and also cases which were very difficult/impossible to analyze via MCSA.

   (iii) Samples of abnormal mechanical load dynamics downstream of the motor.

2. The case histories are deliberately presented in great detail so that practitioners of MCSA understand the complexity of making a final decision as to whether an induction motor actually has or has not a cage winding break, or an abnormal level of operational airgap eccentricity or that a problem may exist in the drive train downstream of the motor causing reflections back into the cage rotor.
3. Each case history is different with a variety of new and practical knowledge being presented.
4. As appropriate, the strengths and weaknesses of MCSA are also covered, particularly in the industrial case histories, since failed diagnoses have to be recognized as being as important as successful ones. Failures in diagnosis, when understood and properly interpreted, alert exponents of MCSA to conditions, which render the identification of fault current signatures impossible or at least very difficult.
5. The industrial case histories have been accumulated by the authors during the past 34 years (as of 2016) from their combined knowledge and experience of the installation, maintenance, design, operation, and condition monitoring of induction motors.
   (i) Published papers by academia have indicated that shorted turns in stator windings and bearing defects in roller element bearings in 3-phase SCIMs can be diagnosed via current monitoring and research papers are referenced on these topics in Chapter 12. However, the application of MCSA in industry to detect these faults in 3-phase SCIMs has not come to fruition in comparison to the widespread usage by end users of MCSA for diagnosing cage winding breaks and operational airgap eccentricity.
   (ii) The authors do not apply current monitoring in industry to detect shorted turns in stator windings or bearing faults in roller element bearings in 3-phase SCIMs for very good reasons, which will be explained and justified in Chapter 12.

The manufacturers of induction motors do not normally release design details of their motors to end users or condition monitoring companies since they have to protect their intellectual property (IP) in a highly competitive market place. Without that complete design information, it is therefore impossible to calculate a definitive magnitude of current components, which are a function of the severity of broken rotor bars or level of airgap eccentricity. During MCSA testing of induction motors in industry, the test engineer has no control over the operating conditions and load currents of the motors being tested and has to accept the actual load on the motor at the time of testing, since plant operators are very reluctant indeed to alter their process to provide a different load current (e.g., full-load amperes). This can be a significant constraint on the application of MCSA in industry.

This is distinctly different from MCSA testing of small induction motors in a laboratory, under controlled conditions, for research results. The core of an MCSA diagnostic strategy and the industrial case histories presented in this book are as follows:

(i) Identify unique current signature patterns (frequency content) indicative of the problem, using proven theoretical principles and frequency equations.

(ii) Estimate the possible seriousness of the problems based on the authors' experience of analyzing MCSA data from thousands of induction motors. This experience is also supported by fundamental research and industrial application papers by the authors, Thomson et al. [1.6 to 1.36] and Culbert et al. [1.37 to 1.42].

Section 6.4 summarizes, with respect to reliable diagnosis of broken rotor bars, all the additional factors which need to be considered before making a final diagnosis and recommendation for the action to be taken by the end user. This information follows on at the end of Chapter 6 on the diagnoses of cage winding breaks, which have been presented in Chapters 5 and 6 and the reader has had the opportunity to consider the practicalities underlying these recommendations. There is also an appraisal in the last chapter that covers successes, external constraints/weaknesses, and lessons learned on the application of MCSA by the author of this chapter, which spans 34 years and also 15 years by Ian Culbert.

1.1 HISTORICAL DEVELOPMENT OF MCSA AND GOALS OF THIS BOOK

In the late 1970s to mid-1980s, novel and fundamental research and development work was simultaneously initiated in the United States, United Kingdom, and mainland Europe on the study of current (and spectra) as a function of cage winding breaks in induction motors. In the United States, this work was reported by, for example, Kliman et al. [1.43, 1.44] and in the United Kingdom and mainland Europe various researchers reported on this topic, including, Williamson, [1.45], Vas [1.46], Deleroi [1.47], Hargis et al. [1.48], Tavner [1.49], Filipetti et al. [1.50], and Thomson [1.34]. In 1982, Thomson initiated research into the diagnosis, via MCSA, of unacceptable levels of operational airgap eccentricity in large HV induction motors operating in power stations and offshore oil production platforms and was the first to report an industrial case history in 1986, when an airgap eccentricity problem was diagnosed [1.37].

With advances in digital signal processing, in the late 1970s, it became possible to produce accurate current spectra of the electrical current to the motor and thus diagnose current signatures indicative of cage winding breaks or abnormal levels of airgap eccentricity between the rotor and stator. Both these problems can lead to consequential stator winding and core damage and failures. Although spectrum analyzers and commercially available MCSA instruments can produce current spectra, which present information pertaining to a cage winding break or abnormal airgap eccentricity and are now widely used by industry, it has to be recognized that such instruments are measurement tools to provide current spectra as the initial source of information to be subsequently interpreted as to whether a problem may or may not exist.

It is important to appreciate that MCSA *"cannot distinguish"* between broken rotor bars and a broken end ring and it certainly cannot identify the position in the cage winding where there is a broken bar. In practice this is not required by industrial

end users, since they are only interested in the operational integrity of cage windings in induction motors and whether there is truly a cage winding break that can lead to a motor failure and downtime. When an MCSA instrument indicates that broken rotor bars exist, it cannot deliver a decision on the action to be taken by the end user and it is here, via the case histories, that this book provides the knowledge to assist end users in decisions on the action to be taken to prevent a catastrophic failure.

To achieve that goal, a combination of expert abilities is necessary for reliable diagnoses; these range over the acquisition and interpretation of the current spectra, which includes digital signal processing knowledge, estimation of the severity of the problem, technical appraisal of the rotor cage design, appreciation of the operational modes of the motor, and very importantly, previous experience, via case histories, of the detection of cage winding breaks or abnormal airgap eccentricity. Interpretation of that information and determination of the required action can be supported by reference to appropriate case histories in this book. Knowledge is also required to enable a risk assessment of the probability of either a stator winding failure caused by cage winding breaks or a rotor to stator rub caused by an airgap eccentricity problem and whether it is safe to continue running the motor. These are the key aptitudes required by engineers, when advising plant managers, so that correct decisions are made. Some of the possible questions and/or decisions depend on the estimated severity of the problem, such as a cage winding break, and how vital the motor is to the end user's production process, and samples of these are now given.

(i) Let it run and minimize the number of direct-on-line (DOL) starts.

(ii) Is there a potential safety hazard if the motor is kept running and what consequential damage could be done, due to, for example, broken rotor bars?

(iii) Whether to stop a motor to prevent a possible catastrophic failure?

(iv) Is it possible to carry out a boroscope inspection while the motor is *in situ*?

(v) Plan a shutdown for repairs as soon as possible.

(vi) Order spare parts, such as new rotor bars and end rings, or even a new rotor.

Consequently, this book is focused on providing a knowledge source for industrial engineers, who are responsible at various levels for the operation, maintenance, and condition monitoring of induction motors driving strategic mechanical plant. This book should be of interest to motor manufacturers (OEMs) and electric motor repair shops, since certain end users are now requiring MCSA tests on brand new motors and after repairs to a SCIM to provide base-line current spectra for comparisons with future on-site MCSA measurements. The OEMs and motor repair workshops should also find MCSA a useful test for *their own internal QA/QC checks* to estimate the operational condition of a cage winding and operational airgap eccentricity during a full-load heat run. However, this would not be part of a Factory Acceptance Test unless there was a formal contractual agreement to so do.

The application of MCSA as part of an overall condition monitoring methodology for strategic SCIMs, is certainly not simply a matter of pressing buttons on an instrument and hoping for a reliable and definitive diagnosis of the actual problem. It

demands more than that and an engineer who intends to apply MCSA should obtain the following competencies:

1. The ability to correctly understand the principles of operation of a 3-phase induction motor during normal operation and to correctly apply the basic equations which are required for MCSA testing.
2. An understanding of the basic construction of large SCIMs.
3. An understanding of the implications of DOL starts, the torque versus speed curves of the SCIM and its mechanical loads and how to calculate, for example, the run-up time of the motor when driving a mechanical load such as a compressor or pump. This initially receives attention in Section 1.3 and in more depth in Chapter 3 because many of the industrial case histories presented in Chapters 5 and 6, in which MCSA detected broken rotor bars, were due to the following:
   - Too many sequential (DOL) starts causing inherent high starting currents, outwith the motor's design capabilities, Richard Nailen [1.51, 1.52], for example, when the end user does not abide by the original manufacturer's (OEM's) specification for the time delays between sequential starts.
   - Incorrect matching of the motor's torque–speed curve to the torque–speed curve of the load, so that there is insufficient accelerating torque to cope with all the starting conditions, to which the motor may be subjected by the end user.

These include the effect on the torque–speed curve of the motor and a consequential reduction in the available accelerating torque, due to voltage dips during a DOL start, for example, on an offshore oil production platform, which has an isolated generating system. Also the effect of starting the motor against an open valve set up in a centrifugal pump which has a greater torque versus speed demand compared to starting against a closed valve system when the SCIM was designed for the latter. This can happen when the end user has not specified all the possible starting conditions (normal and abnormal) to the manufacturer of a SCIM.

Numerous papers by other researchers and industrial engineers, which are relevant to MCSA will be referenced in due course, but only where applicable to the specific context and content of the particular chapter, and furthermore it is impossible to list all the publications on this subject. A Bibliography in an IEEE Transactions paper by Benbouzi [1.53] lists 372 references on *Induction Motor Faults Detection and Diagnosis* covering various diagnostic techniques and is an excellent source for published papers.

1.2 BASIC THEORY OF OPERATION OF THE 3-PHASE INDUCTION MOTOR

There are many text books on electrical machines, and a sample of these include, El-Hawary [1.54], Liwschitz and Whipple [1.55], Say [1.56], Sen [1.57], Chapman

[1.58], Hughes [1.59], and Slemon [1.60], which contain the theory of operation of a 3-phase squirrel cage motor. There are also specialist books dedicated solely to induction motors by, for example, Phillip Alger on "The Nature of Induction Machines" [1.61] and an older but excellent book by Herbert Vickers on "The Induction Motor" [1.62]. These particular books have been referenced since they provide an excellent and comprehensive treatment of the induction motor that covers, for example, the theory of operation of an induction motor, starting characteristics, 3-phase winding theory, design and construction of induction motors, unbalanced magnetic pull, slot combinations, magnetic noise and vibration, testing, and the industrial application of induction motors.

The style of presentation in Sections 1.2 and 1.3 is hopefully suited to the needs of electrical, mechanical, maintenance, and condition monitoring engineers and also chief electricians and senior technicians working in industry, who are responsible for the maintenance and condition monitoring of 3-phase induction motors. It is not the intention to merely regurgitate information, on the operation of the induction motor, which is already in the aforementioned books. The content that follows is deliberately written to avoid being over theoretical and contains the minimum of mathematics since this is not a classical style text book for academia and students, but nevertheless, it should be of interest to graduate and inexperienced engineers working with induction motors in a wide range of industries.

The 3-phase induction motor produces torque and power at the output shaft due to the combination of three fundamental phenomena and these are

(i) The production of a rotating magnetic field from a 3-phase winding supplied by a 3-phase supply voltage—Tesla's rotating magnetic field principle.

(ii) An electromotive force (emf) is induced in a coil placed in a changing, in this case, rotating magnetic field—Faraday's law of electromagnetic induction.

(iii) A current carrying coil placed in a magnetic field experiences a force—Oersted and Faraday's experiments.

The mathematical proof that a 3-phase balanced voltage (each phase spaced 120 degrees apart) supplied to a balanced 3-phase stator winding (with each phase spatially distributed 120 degrees apart) produces a rotating magnetic field in only one direction, can be found in numerous text books on electrical machines [1.54–1.62] and will not be repeated in this book. A stator core, into which the 3-phase winding is inserted, is made of high quality, electrical steel laminations to reduce eddy current losses [1.56, 1.61, 1.62], these laminations are insulated from each other and a photo of part of an unwound stator core assembly is shown in Figure 1.1.

Examples of stator core assemblies for large HV SCIMs are shown in Figures 1.2 and 1.3 with the HV windings inserted and Figure 1.3a is a sectioned view of a 3-phase induction motor. The coils are inserted into the stator core slots and the insulation on the coils is designed to suit the applied voltages, full details of insulation types for stator coils and coil shapes can be found in the book by Stone et al. [1.3].

A 3-phase induction motor cannot deliver power and torque solely due to the fact that a 3-phase winding supplied by a 3-phase balanced voltage supply produces a rotating magnetic field, Tesla [1.1]. To achieve output torque and power at the shaft

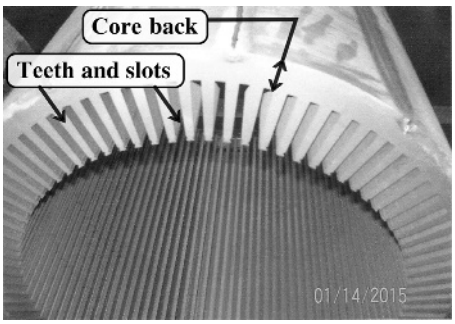

Figure 1.1 Example of an unwound stator core. Reproduced with permission of Nidec Corporation, US Electric Motors Division.

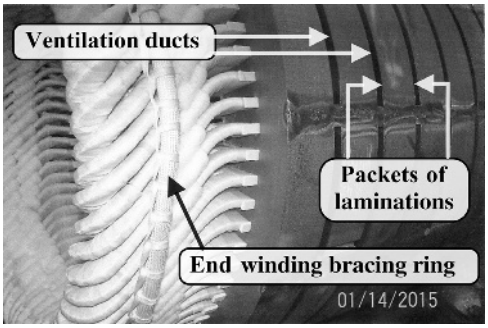

Figure 1.2 HV winding inserted into the stator core. Reproduced with permission of Nidec Corporation, US Electric Motors Division.

requires the application of the second phenomenon, namely, Michael Faraday's discovery of electromagnetic induction which is *"that an electromotive force (emf) will be induced in a coil due to the rate of change of flux linking that coil"* and he demonstrated and presented the phenomenon to the Royal Society in the United Kingdom on November 24, 1831, Dunsheath [1.65]. Faraday carried out a series of experiments

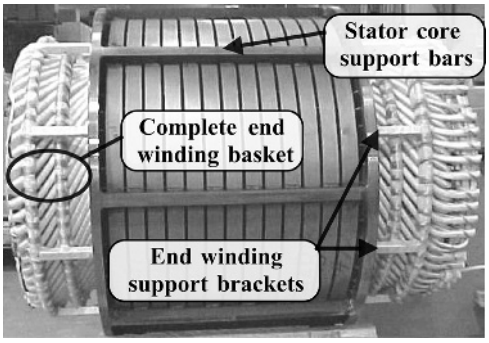

Figure 1.3 Complete HV stator core assembly. Reproduced with permission of Baldor Electric Company, USA, a member of the ABB group.

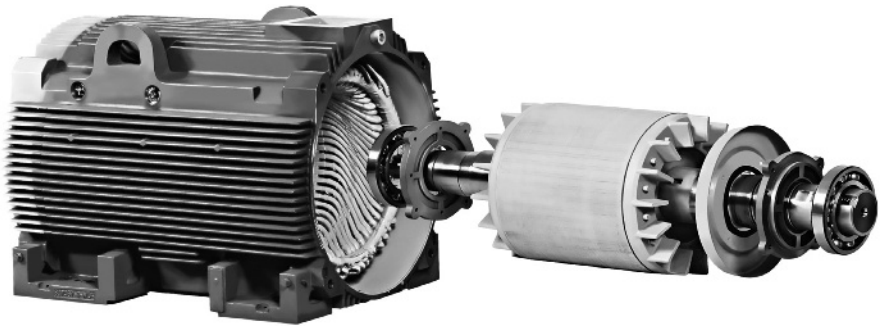

Figure 1.3a Sectional view of 3-phase SCIM. Reproduced with permission of Baldor Electric Company, USA, a member of the ABB group.

that led to this famous discovery of electromagnetic induction during a very short period of 10 days [1.64] in 1831, but it is quite incorrect to think that this was a spontaneous result, since this was after many years of dedicated research, experimentation on electric currents and magnetism and their interaction. A list of Faraday's diaries, and other references is given in Reference 1.65. Faraday's discovery at that time, was a truly remarkable achievement, by an experimenter, and may be considered to be one of the most important discoveries in electrical engineering, which produced by one individual, shaped the world as we know it today. For example, the generation of electricity is dependent on Faradays' law of electromagnetic induction and for completeness it is presented mathematically.

$$e = -N_T d\phi/dt \text{ volts} \tag{1.1}$$

e = instantaneous magnitude of the electromagnetic force (emf) in volts

N_T = number of turns

ϕ = magnetic flux in webers

t = time in seconds

The negative sign indicates that a current flowing in response to the induced voltage (e) produces a magnetic field opposing the original field (Lenz's law). When a set of open circuited conductors is placed in a rotating magnetic field and inserted into a laminated, magnetic steel rotor core in the stator bore of a stator winding assembly shown in Figure 1.4, then by Faraday's law, an emf will be induced in these conductors.

The loop has been closed on the second phenomenon that leads to an induction motor being able to turn and produce torque. However, at this stage, the rotor will not turn, since the induction motor is simply a transformer whose primary winding is the stator and its secondary winding is the open circuited conductors in the rotor, inserted into the stator bore.

Now consider the third phenomenon, Hans Oersted, on April 21, 1820 observed that a compass needle moved from its magnetic North, when an electric current (supplied by a battery) passed through a wire close to the compass needle, and crucially, it only moved when the current was switched *"on and off."* Michael Faraday repeated

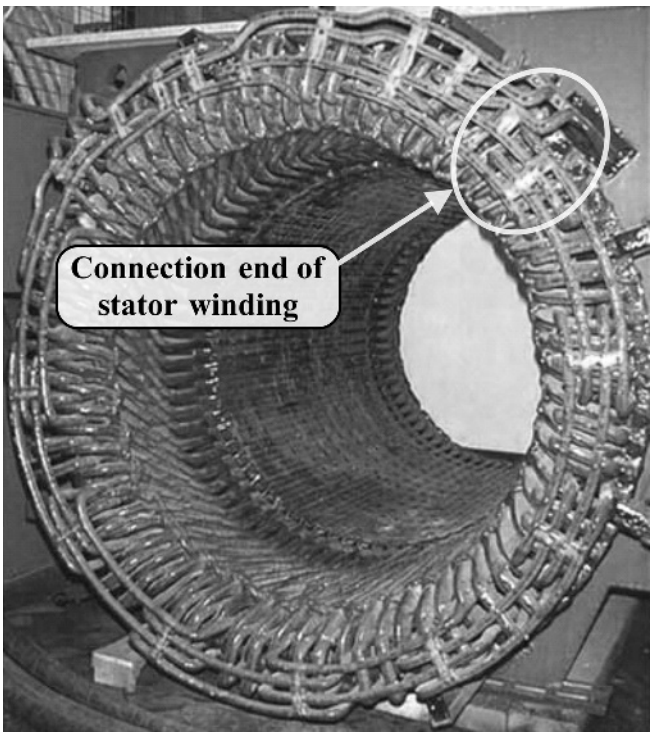

Figure 1.4 3-phase HV stator winding assembly.

Oersted's experiments but also found that a magnet exerts a force on a wire carrying an electric current. Thus if the conductors in the stator bore carry current in a rotating magnetic field they will experience a force. This can be achieved by simply short circuiting the conductors and Faraday's induced emfs will drive currents through them. The final step has been explained since these conductors will turn and produce torque.

The practical fruition of a set of current carrying conductors is achieved by using a set of copper bars, which are joined (via brazing or induction heating) to short circuiting end rings as illustrated in Figure 1.5. The copper cage winding is installed into a laminated rotor core by first inserting the rotor bars into the core and by then brazing or welding the bars to the end rings. Figures 1.6 and 1.7 give examples of squirrel cage rotors.

Each rotor bar in the cage winding experiences, in the direction of the rotating magnetic field, a force which is transferred to the rotor core structure. The rotor then rotates and produces torque and power output. The principles of operation of a 3-phase induction motor can be summarized as follows:

> "*In the induction motor there is a rotating electromagnetic field from the 3-phase stator winding and by Faraday's law emfs are induced in the rotor conductors, which drive currents through the short-circuited cage winding, and the cage winding experiences a force since it is carrying current in a rotating field.*"

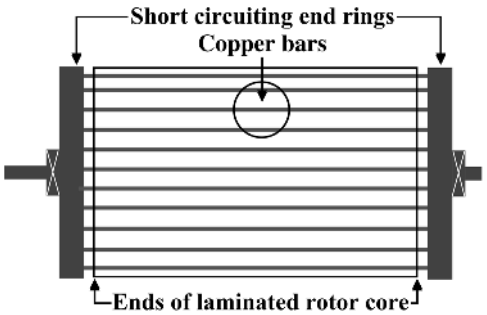

Figure 1.5 Schematic illustration of a squirrel cage copper or aluminum fabricated winding.

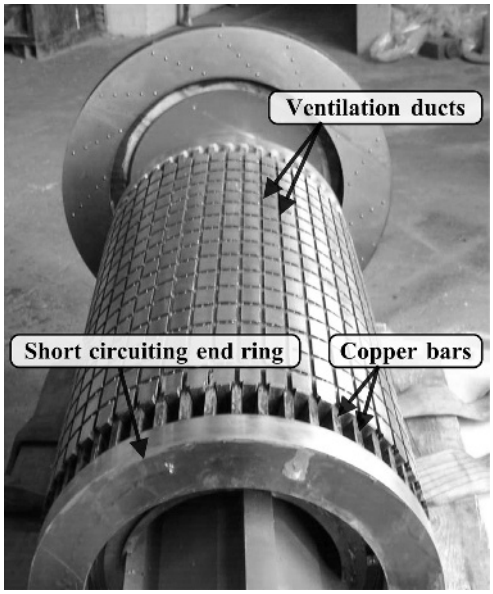

Figure 1.6 Copper fabricated squirrel cage rotor.

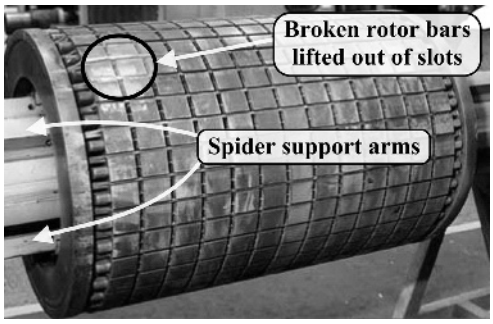

Figure 1.7 Squirrel cage rotor with a broken rotor bar that has lifted. *Source:* Thomson and Fenger [1.13]. Reproduced with permission of IEEE.

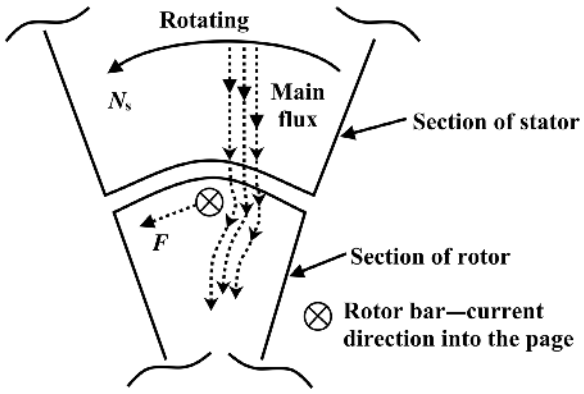

Figure 1.8a Induction motor action.

Figure 1.8a is an illustration of the force and torque on a cage rotor due to the interaction between the main flux (at synchronous speed, N_s), which links the induced currents in the rotor bars. The direction of force/motion is in the tangential direction and is obtained via Fleming's left hand rule for motoring action.

- The **F**irst finger is the direction of **F**lux from the stator to the rotor.
- The se**C**ond finger is the direction of **C**urrent.
- The thu**M**b is the direction of the **M**otion.

These three fingers are mutually perpendicular to each other.

Hopefully the style of the explanations will meet its objectives, namely to integrate theoretical principles supported by examples of practical implementation. As a visual aid to understanding, a finite element plot of the distribution of the magnetic field for an 8-pole induction motor is shown in Figure 1.8b and in Figure 1.9 the lines of magnetic flux are clearly shown. These follow the paths of least magnetic

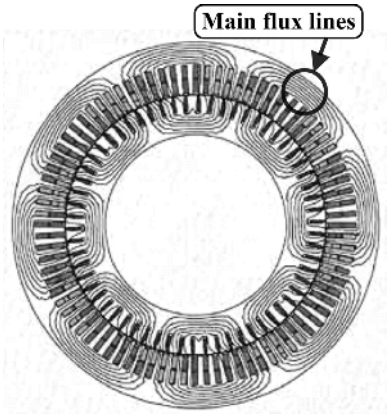

Figure 1.8b Finite element plot of distribution of magnetic field in an 8-pole induction motor. Reproduced with permission of EM Diagnostics Ltd.

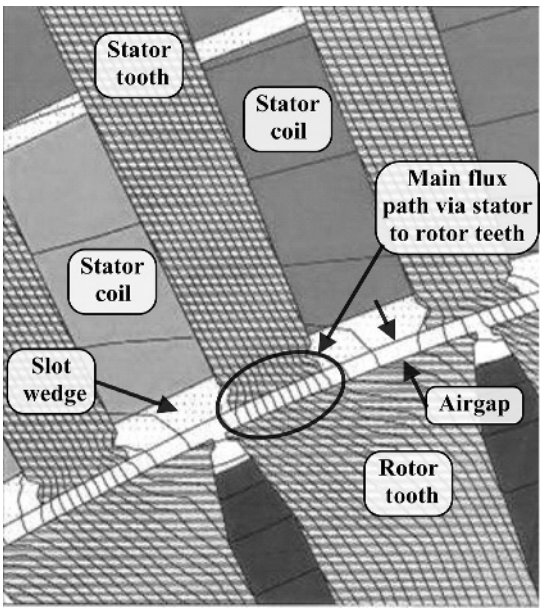

Figure 1.9 Finite element model showing the magnetic flux lines taking the path of least magnetic reluctance through the stator and rotor teeth to cross the airgap. Reproduced with permission of EM Diagnostics Ltd.

reluctance* (opposition to flow of flux*), via the stator and rotor teeth, to cross the air gap and link the rotor cage winding, as opposed to the higher reluctance route via the stator and rotor slots. Leakage flux lines from the main flux paths do of course diverge into the stator and rotor slot regions as specifically shown in Figure 1.9.

The construction and design features of different types of squirrel cage rotor are fully covered in Chapter 2 of this book while the forces and stresses that a cage winding experiences are presented in Chapter 3.

The use of the name squirrel in squirrel cage rotor comes from a rotating cage, which was sometimes used in the United States for squirrels as an external exercise aid and since the animal is fast and agile it was a very appropriate name to give to the cage rotor. The Westinghouse Corporation (who bought the rights from Tesla on his patents of the induction motor) in the United States was the first company to manufacture induction motors on an industrial scale. On a light hearted note, in the United Kingdom the same form of cage was used to provide pet mice with an exercise aid. Clearly the use of squirrel, in squirrel cage rotor, is much more elegant than the use of a "*mouse*" cage rotor.

1.2.1 Key Equations for MCSA Based on Operation of a 3-Phase Induction Motor

The 3-phase winding on the stator is supplied with a balanced 3-phase voltage supply at a certain frequency and is wound to produce a forward rotating magnetic field with a specific number of poles. The equation that relates the fundamental supply frequency

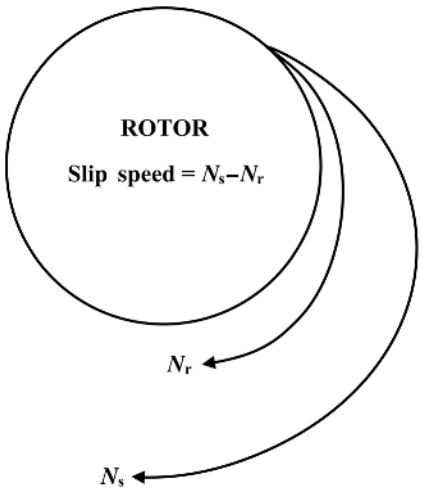

Figure 1.10 Illustration of slip speed in r/min.

f, of the voltage supply to a 3-phase stator winding and the synchronous speed N_s (r/min) of the rotating magnetic field produced by the stator winding of pole-pairs p, is given by

$$f = N_S p/60 \quad \text{Hz} \tag{1.2}$$

where

N_s is in r/min

p = pole-pairs

The rotor rotates at a speed of N_rr/min as illustrated in Figure 1.10 and the diagram shows that, to supply the load torque, the rotor always rotates at a speed less than the synchronous speed. A measure of the slipping back of the rotor is termed the slip and is given by

$$s = (N_s - N_r)/N_s \tag{1.3}$$

This is a per unit term with the synchronous speed being the base reference speed and the slip normally given as a percentage.

The slip speed, which equals $N_s - N_r$ is the actual difference in r/min between the speed of the rotating magnetic field from the stator winding and the actual speed of the rotor but note that the definition of "slip frequency" is not the slip speed $N_s - N_r$ divided by 60 to convert to hertz. The term slip frequency in induction motor theory [1.54–1.62] has a specific electrical meaning, which is the frequency of the rotor currents and is given by

$$f_2 = (N_s - N_r)p/60 = sN_s p/60 = sf \quad \text{Hz} \tag{1.4}$$

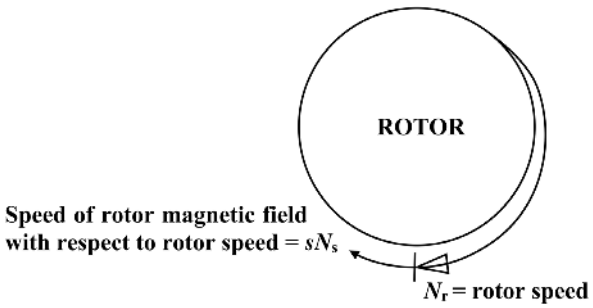

Figure 1.11 Illustration of forward rotating field N_{fr} from rotor currents.

$f_2 = sf$ = slip frequency in hertz of induced emfs and currents in the cage winding.

This is the correct terminology for slip frequency but unfortunately a considerable number of condition monitoring companies who offer MCSA monitoring services, particularly those whose main services are in vibration monitoring, have incorrectly defined slip frequency as being equal to $(N_s - N_r)/60$ Hz. The forward rotating magnetic field, defined by N_{fr} and produced by the rotor currents with respect to a fixed position on the rotating rotor moves faster than the actual rotor speed as illustrated in Figure 1.11 and is at a speed of

$$N_{fr} = N_s - N_r = sN_s \tag{1.5}$$

The speed of the forward rotating magnetic field produced by the current carrying rotor conductors with respect to the stationary stator winding is given by

$$\text{Rotor speed } N_r + \text{Rotor field speed } sN_s = \text{Synchronous speed}$$
$$N_r + sN_s = N_r + N_s - N_r = N_s$$

With respect to a stationary observer on the fixed stator winding, the speed of the rotating magnetic field from the rotor equals the speed of the stator rotating magnetic field, namely, the synchronous speed, N_s. This has to be the case and it is an important result but initially it can be somewhat challenging to understand. Both fields must be locked together to give steady torque production from an induction motor.

1.2.2 Interpretation of Motor Nameplate and Application of Basic Equations

It is now logical to interpret the nameplate data on a 3-phase induction motor, with particular reference to the application of MCSA, since that is the first step in carrying out the measurement of current and analysis of the current spectrum. Typical information on the nameplates of SCIMs manufactured for the UK and US markets is shown in Figures 1.12 and 1.13, respectively. It is often the case that the relevant nameplate data from SCIMs is not fully recorded in condition monitoring reports and this perhaps suggests that it is not appreciated how much useful information can

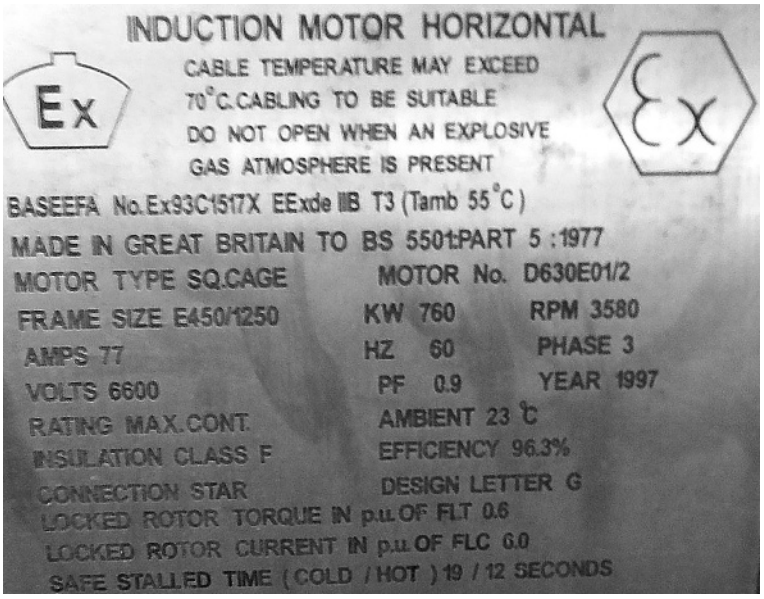

Figure 1.12 Nameplate from a 6.6 kV, 760 kW/1018 HP, 60 Hz SCIM.

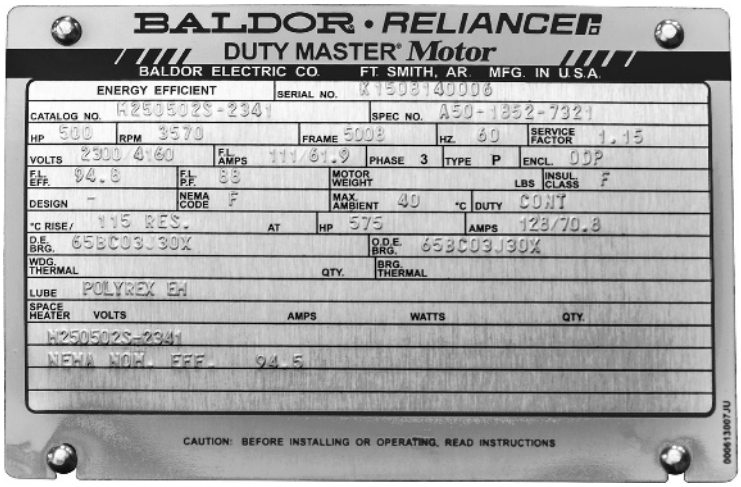

Figure 1.13 Photo of a nameplate from a 4160 V, 500 HP/373 kW, SCIM, reproduced by kind permission of © Baldor Electric Company, USA, a member of the ABB group.

be obtained and calculated from that data. It is the authors' experience that far too little attention is given to the interpretation of the nameplate, particularly by young and recently graduated electrical engineers, who have studied electrical engineering but may well be unsure of the actual meaning of the data thereon. It is important to stress the importance of that data and to comment on what is relevant information for MCSA.

The inclusion of this section on nameplate information is not about the total content of an induction motor's nameplate, since that is the domain of the manufacturers and the various standards, such as NEMA MG1 [1.66]. However, the only comment the authors wish to make to motor manufacturers in a worldwide context is that it would be extremely helpful to the end user and for the application of MCSA to stamp the number of rotor slots on the nameplate.

The information on the nameplates of motors manufactured for the US market is normally governed by the specifications of NEMA MG1 [1.66], and these requirements include

(a) Manufacturer's type and frame designation
(b) Horsepower output
(c) Time rating
(d) Temperature rise
(e) r/min at rated load
(f) Frequency
(g) Number of phases
(h) Voltage
(i) Rated-load amperes
(j) Code letter (see Section 20.9 in Reference 1.66)
(k) Service factor

Induction motors manufactured in the United Kingdom and on mainland Europe use kW for the power output at the shaft and N·m for Torque, whereas in the United States the units HP and lbsf·ft are used. The information on the nameplate nominally means that, when the motor is supplied at the rated volts and frequency and appropriately loaded it will deliver a full-load rated output power at the shaft in HP or kW and at the speed on the nameplate. The input current and power factor will also be the full-load rated values.

The nameplate of an HV SCIM manufactured in the United Kingdom, is shown in Figure 1.12 and as per normal, it does not give the number of poles, synchronous speed, operating slip s_{FL}, or the full-load rated torque. It is often the case that OEMs of large, HV SCIMs in the United Kingdom, stamp on the nameplate, the locked rotor torque and locked rotor current in per unit or percentage quantities of the full-load torque (FLT) and full-load current (FLC). Although the following may well be considered to be obvious to electrical power engineers, recall that MCSA is also used by non-electrical power engineers, thus it is important to explicitly explain the meaning of information on the nameplate which is relevant to MCSA.

With respect to Figure 1.12

$$\text{Power output at the shaft } P = 760\,\text{kW or } 1018\,\text{HP}$$

Since the full-load efficiency is given the electrical power input is

$$P_{\text{in}} = 760/0.963 = 789\ \text{kW}$$

For completeness, recall power input $P_{\text{in}} = \sqrt{3}V_{\text{L}}I_{\text{L}}\cos\phi$

The full-load rated speed is 3580 r/min and on a 60 Hz supply the synchronous speed in r/min of the rotating magnetic field from the stator winding of a 2-pole (pole-pairs, $p = 1$) motor is

$$N_{\text{s}} = (3600)/p = 3600\ \text{r/min}$$

And since the rated full-load speed is 3580 r/min, which is just below 3600 r/min it is a 2-pole motor. The full-load slip, $s_{\text{FL}} = (N_{\text{s}} - N_{\text{r}})/N_{\text{s}} = 0.0055$ or 0.55% at a nominal full-load rated speed of 3580 r/min.

The full-load slip is the first reference information that is required for MCSA, it is a crucial parameter as verified in Chapter 4. However, SCIMs are often operating below full-load, hence the input current, output speed, and power output will be less than the full-load rated values. At this early stage in the book, it should be mentioned that the nominal full-load speed on the nameplate may not be that which occurs in practice and the implications of this with respect to MCSA testing will be discussed in more detail in the case histories in Chapters 5 and 6.

The frequency of the currents in the squirrel cage rotor at full-load for this motor is $f_2 = s_{\text{FL}}f = 0.0055 \times 60 = 0.33\text{Hz}$ (close to dc) which is a very low frequency in comparison to the stator supply frequency. At switch on when the slip is 1.0 the frequency of the rotor currents equals the supply frequency.

The nameplate shown in Figure 1.12 does not give the full-load rated torque but this can be calculated from

$$\text{Power output at the shaft } P = \omega T \quad \text{N} \cdot \text{m}$$

$$\text{Full-load torque } T = 760 \times 10^3/((2\pi 3580/60)) = 2027\ (\cong 2000)\text{N} \cdot \text{m}$$

Due cognizance is given to the units used for power output and torque at the shaft used by industry in the United States, which are HP and lbsf·ft and as stated in NEMA MG1, therefore $T = 1496$ lbsf·ft (often stated in lbs·ft by industry but pounds force (lbsf·ft) is the correct unit since lbs is a mass and not a force).

$$1.0\ \text{N} \cdot \text{m} \cong 0.74\ \text{lbsf ft}$$

Two useful formulae for calculating torque but recall 746 W = 1.0 HP

$$T = \frac{(9550 \times \text{Power out in kW})}{\text{Rotor speed in r/min}}\ \text{N} \cdot \text{m}$$

$$T = \frac{(5250 \times \text{HP})}{\text{Rotor speed in r/min}}\ \text{lbsf} \cdot \text{ft}$$

(i) Figure 1.12 gives the locked rotor current or starting current presented on the nameplate as being FLC 6.0 which is six times the FLC and gives a starting current (I_{s}) of 462 A. Thus the cage winding is subjected to high mechanical

TABLE 1.1 Relationships Between Frequency, Poles, Rotor Speed, Slip, and Frequency of Rotor Currents

Mains Supply Frequency	Poles	Synch. Speed of Stator Rotating Field	Rotor Speed Variable	Slip Depends on Load	Freq. of Rotor Currents
f (Hz)	Number	N_s (r/min)	N_r (r/min)	s	f_2 (Hz)
60	2-poles	3600	3564	1.0%	0.6
50	2-poles	3000	2985	0.5%	0.25
60	4-poles	1800	1782	1%	0.6
50	4-poles	1500	1470	2%	1.0
60	6-poles	1200	1194	0.5%	0.3
50	6-poles	1000	952	0.8%	0.4
60	12-poles	600	590	1.66%	1.0

and electromagnetic forces and high thermal stresses due to temperature being proportional to current squared (I^2). These are discussed in detail in Chapter 3.

(ii) The locked rotor or starting torque (T_s) given on the nameplate is FLT 0.6, which is 60% of the calculated FLT (≅2000 N·m) and is 1200 N·m or 885 lbsf ft.

(iii) Table 1.1 gives sample values of frequency, pole-pairs, synchronous speed, actual rotor speed, slip, and slip frequency of rotor currents for SCIMs.

When an induction motor is supplied at rated volts and frequency and is running on no-load (and uncoupled) the input current consists of two components, which are phasors and therefore cannot be directly added to give a resultant.

(i) The magnetizing current, which sets up the rotating magnetic field lags the supply volts by 90°

(ii) An active component of the no-load current to the motor which is in phase with the supply voltage and supplies the core losses

There can be a misconception in calculating the percentage load at which the motor is operating, when the input current is incorrectly used to give that percentage loading. The power output and shaft speed are not normally measured on SCIMs operating in industry but the input current to large, HV SCIMs is normally continuously measured. This motor actually takes a current of 14 A on a no-load, uncoupled run and that current is part of the input current at any loading of the motor.

- Consider that this motor, which has a FLC of 77 A, is operating at an input current of 40 A. That does not mean that the motor is operating at 52% of its rated full-load power output at the shaft, because a portion of the 40 A provides the constant 14 A no-load mainly magnetizing current which does not contribute to the output power.
- The motor is taking 52% of the rated full-load amperes but that is different from the output power at the shaft and the operating slip is certainly not 52% of the full-load slip. This is an important fact, when applying MCSA and interpreting the current spectrum, as is discussed and demonstrated in Chapter 4.

1.3 STARTING AND RUN-UP CHARACTERISTICS OF SCIMS

There are many publications which cover the reasons for a SCIM taking a large starting current, when started DOL, and these publications also discuss the design features, which can change the starting current and it is not the intention of this book to repeat already published information. The reader is referred to Nailen's papers, [1.51, 1.52], which discuss in detail the starting demands and implications of DOL starting of 3-phase SCIMs for the oil industry but these papers are equally relevant to other industries and are particularly relevant due to the causes of cage winding breaks in a number of the MCSA case histories presented in Chapters 5 and 6. The main focus in this book is on the application of MCSA to motors that are started DOL and Chapter 3, with appropriate references, discusses the forces and stresses on an induction motor during a DOL start.

Suffice to state that a SCIM takes a large starting current, which can be up to six or seven times the rated FLC, when switched DOL, since at the instant of switch on, a SCIM is effectively a short circuited transformer, which inevitably takes a large starting current. The starting current is a function of numerous parameters such as the supply voltage, resistance and reactance of the rotor, the operating flux density and the magnetic circuit, and airgap length in the motor. In addition, the frequency of the voltage and currents in the rotor cage is at the supply frequency at switch on (slip is 1.0 and $f_2 = sf, f_2 = f$). There is the phenomenon known as skin effect [1.55, 1.61, 1.62, 1.63], which causes the current distribution in the rotor bars to be a function of frequency and the ac resistance of the rotor cage winding changes as the frequency changes from the supply frequency at switch on down to nearly dc at steady-state operation. This is fully discussed in Chapter 2. It is the expertise of the electrical machine designer to design the motor to have a specific starting current as specified by the end user, to also suit any limitations of the supply network, to which it will be connected. Also, the motor must have the required torque-speed curve to suit the starting and running requirements from the mechanical load.

Also, a high starting current taken by a large SCIM operating on an offshore oil production platform (an isolated generating system) inevitably causes a voltage dip during start up, which means the available torque from the motor drops since torque is proportional to the voltage squared, V^2. As an illustration, consider the following motor, which was specifically designed to have a relatively low starting current. It was used on an offshore oil and gas production platform, which has its own generators and thus there are restrictions on the starting current to prevent an excessive voltage dip on start up. The motor was driving a reciprocating compressor.

Motor Name Plate Data

3-phase SCIM, 6600 V, 2900 kW/3887 HP 340 A, 60 Hz, 890 r/min, S1, MCR

Locked rotor current 1275 A.

Locked rotor torque 17,113 N·m. (12,630 lbsf·ft)

Breakdown torque 46,674 N·m. (34,445 lbsf·ft)

The FLT is given by

$$T_{FL} = (9550 \times \text{Power output in kW})/\text{Rotor speed in r/min}$$
$$= 9550 \times 2900/890 = 31{,}116\ \text{N} \cdot \text{m}(22{,}931\ \text{lbsf} \cdot \text{ft})$$

The following items (i–iv) were reproduced with permission of Parsons Peebles, Scotland:

(i) Run-up time at 100% volts: Motor + Load = 2.6 seconds

(ii) Total moment of inertia: 350 kg-m^2 (8314 lbs-ft^2)

(iii) Allowable run-up time at 100% volts: 9 seconds from cold, 6 seconds from hot

(iv) Safe stall time at 100% volts: 10 seconds from cold, 7 seconds from hot

The current versus speed curve from switch on is shown in Figure 1.14.

This shows that the current is greater than three times the FLC up to around 90% of synchronous speed. Thus the faster the motor can run up to its steady-state operation the less exposure the rotor bars have to high currents, with their consequential thermal stresses, electromagnetic forces, and mechanical bending stresses on the bars and end rings external to the rotor core ends. To meet the needs of industry, this specially designed motor has a low starting current (3.75 FLC) for a large HV motor. Recall that in Figure 1.12, which gives the nameplate data for a different HV SCIM, the starting current is six times FLC.

The torque versus speed curve for the motor under discussion is shown in Figure 1.15 and all the area under the curve is available for accelerating the motor up to its no-load speed since there is no load on the motor. OEMs normally provide to their customers a torque–speed curve similar to that shown in Figure 1.15. The curve

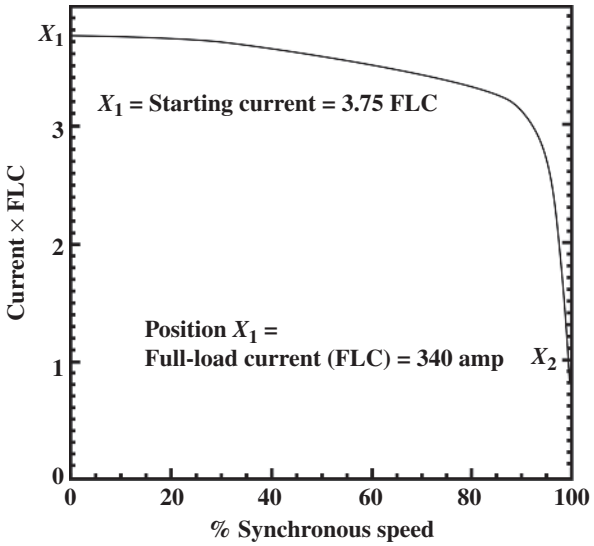

Figure 1.14 Current versus speed. Reproduced with permission of Parsons Peebles, Scotland.

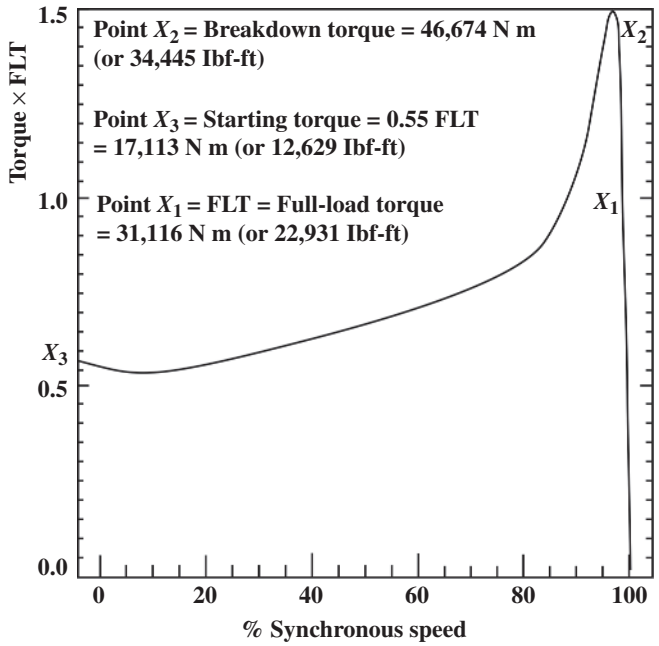

Figure 1.15 Torque versus speed curve for the motor. Reproduced with permission of Parsons Peebles, Scotland.

is non-linear up to a point immediately beyond the breakdown torque (X_2) and cannot be expressed by a single algebraic equation over that speed range but it is linear in the straight line portion (negative slope) of the plot down to the no-load speed (virtually synchronous speed, N_s).

Due to the speed scale used in Figure 1.15, which covers the full speed range, it is not possible to obtain the torque and corresponding speed directly from the plot between N_s and the full-load speed, N_{rFL} (at X_1). It is fully appreciated that the graph in Figure 1.5 between no-load to FLT versus speed can be redrawn to a different scale whereby the torque at different speeds between no-load and full-load can be read directly from a new graph. However, this requires the end user to do so and to avoid this the following analysis shows that it is unnecessary. The objective of the following analysis is to

(i) Provide a simple equation to calculate the torque at any speed (N_r) or vice versa from the linear part of the graph between no-load and full-load at position X_1.

Figure 1.15a is obtained from Figure 1.15 but with speed on the y-axis and torque on the x-axis to focus on the speed–torque curve between N_s and the full-load speed and torque. The graph shown in Figure 1.15a can be represented by the very simple equation that describes a straight line curve, namely $y = mx + c$.

In this case the y-axis is the speed (N_r), m is the slope of the curve, which is negative in this case (speed drops as torque increases), the x-axis is torque, and c is

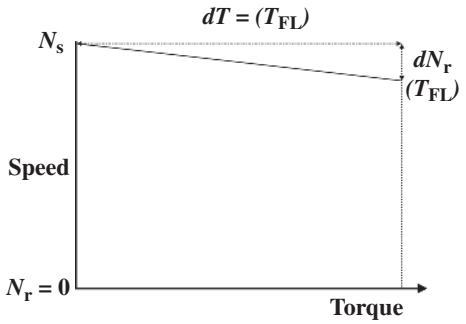

Figure 1.15a Speed versus torque for the operating region between no-load and full-load.

the intercept on the *y*-axis, which is the synchronous speed (N_s). The equation for the graph on Figure 1.15a is therefore

$$N_r = \left[\left(-\frac{dN_r}{dT}\right) T\right] + N_s \tag{1.6}$$

Equation (1.6) can be rearranged into a more convenient form

$$T = \left[\frac{(N_S - N_r)}{(N_S - N_{rFL})}\right] T_{FL} \tag{1.6a}$$

The operational slip $s_o = \dfrac{(N_S - N_r)}{N_S}$

The full-load slip $s_{FL} = \dfrac{(N_S - N_{rFL})}{N_S}$

Rearranging equation (1.6) gives

$$\frac{T_{FL}}{T} = \frac{s_{FL}}{s_o} \tag{1.7}$$

The torque is therefore proportional to slip in the linear region of the torque–speed graph.

Where

N_s = synchronous speed, r/min

N_r = speed at any torque between synchronous speed and the speed at full-load torque, r/min

N_{rFL} = speed at full-load, r/min

dN_r = change in speed between synchronous speed and full-load speed, $(N_s - N_{rFL})$, r/min

T = torque at any speed between N_s and N_{rFL}, N·m (lbsf·ft)

T_{FL} = full-load torque, N·m (lbsf·ft)

dT = change in torque between torque (zero) at synchronous speed and T_{FL}, N·m (lbsf·ft)

Example The torque–speed curve in Figure 1.15 is for a 3-phase, 6600 V, 2900 kW/3887 HP, 340 A, 60 Hz, 890 r/min SCIM. The FLT was previously calculated from the nominal full-load rated speed and power output (nameplate data) and is 31,116 N·m. The synchronous speed is 900 r/min and the full-load speed (nameplate data) is 890 r/min. Calculate the operating torque at a speed of 894 r/min.

$$\text{From equation (1.6a) } T = \left[\frac{(N_S - N_r)}{(N_S - N_{rFL})}\right] T_{FL} = \left[\frac{(900 - 894)}{(900 - 890)}\right] 31{,}116 = 18{,}670 \text{ N m}$$

$$\text{Or from equation (1.7) } T = \left(\frac{s_o}{s_{FL}}\right) T_{FL} = \left(\frac{0.0067}{0.011}\right) 31{,}116 = 18{,}670 \text{ N m}$$

The answers are equal and prove that the torque for a 3-phase SCIM is proportional to slip (equation 1.7) in the steady-state operating region between full-load and no-load.

1.3.1 Calculation of Run-Up Time of SCIM Driving a Mechanical Load

It is assumed that the windage and friction torques are negligible. The area between the two curves in Figure 1.16 is the accelerating torque available to accelerate the motor up to the steady-state operating speed demanded by the mechanical load. This occurs at the cross over point in Figure 1.16 between the two curves, provided that

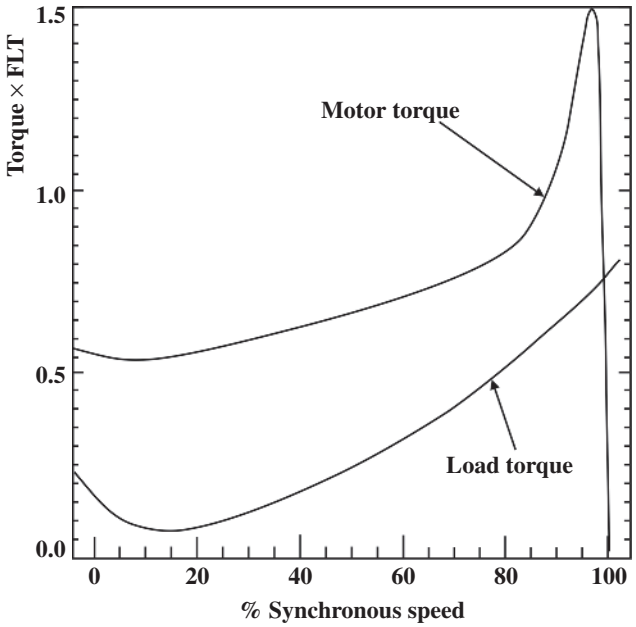

Figure 1.16 Torque versus speed curves for the motor and load. Reproduced with permission of Parsons Peebles, Scotland.

the cross over occurs in the negative slope of the motor's torque curve, in which case steady state will be obtained.

Torque required from the motor to drive the load is given by (and using metric units)

$$T_{\mathrm{m}} = T_{\mathrm{ma}} + T_{\mathrm{L}}$$

T_{m} = total torque from motor, N·m

T_{ma} = accelerating torque to start the motor and overcome its inertia (J), N·m

T_{L} = load torque, N·m

A step–by-step mathematical integration solution can be used to calculate the run-up time. The accelerating torque is

$$T_{\mathrm{ma}} = J(d_{\mathrm{wr}}/d_{\mathrm{t}})$$

$$\int dt = J/T_{\mathrm{ma}} \int_{wr_1}^{wr_2} d_{\mathrm{wr}}$$

$$t = (J/T_{\mathrm{ma}})(w_{\mathrm{r2}} - w_{\mathrm{r1}}) \tag{1.8}$$

If small steps in $d_{\mathrm{wr}} = w_{\mathrm{r2}} - w_{\mathrm{r1}}$ are taken, it is assumed that the curve is linear during each step, therefore the time for the motor to accelerate in that period can be calculated. The smaller the step in d_{wr} the more accurate is the assumption of linearity. In this illustration only 20 steps are shown in Figure 1.17 but the greater the number of steps of d_{wr}, the more accurate is the result for the total run-up time (t). The average accelerating torque is taken directly from the curves and the Δt time is determined between the two curves as shown in Figure 1.17. All the Δt times are then used to plot the run-up time versus the speed from zero up to the steady-state speed. In this illustration, for this 8-pole motor and reciprocating compressor the total inertia is taken to be 350 kg-m^2 (8314 lbs-ft^2).

Using Metric Units

From Figure 1.17, each step is 45 r/min, $d_{\mathrm{wr}} = 2\pi 45/60 = 4.7\mathrm{rad/sec}$

The time to accelerate between each step is given by

$$\Delta t = (J/T_{\mathrm{av}})(w_{\mathrm{r2}} - w_{\mathrm{r1}})$$

A sample calculation for Δt_1 for the first step between zero speed to 45 r/min (i.e., $d_{\mathrm{wr}} = 4.71\,\mathrm{rad/sec}$) the average accelerating torque (T_{av}) between the two curves is 12,466 N·m.

$$\Delta t_1 = (350/12{,}466)(4.7) = 0.13\,\text{seconds}$$

Using Imperial units, Dymond [1.64]

Δt = the time taken to accelerate during the selected step ΔS in r/min is given by

$$\Delta t = \frac{\left(WK^2M + WK^2DE\right) \times \Delta S}{308 \times (Ta)}\ \text{seconds} \tag{1.9}$$

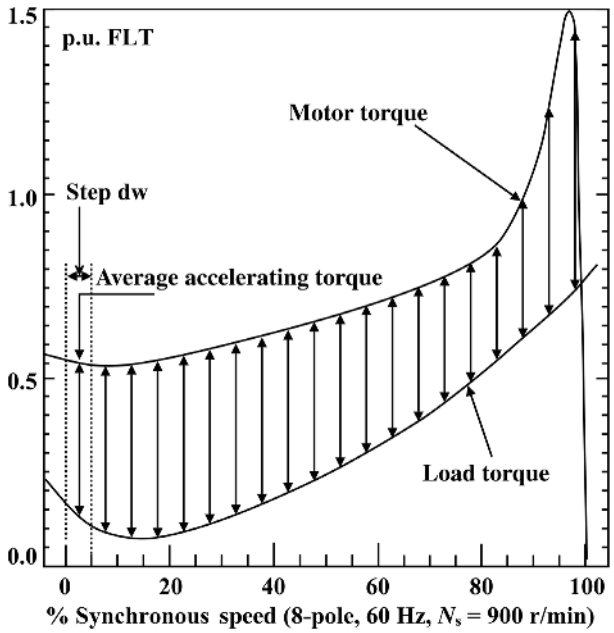

Figure 1.17 Per unit torque versus percentage of synchronous speed—step-by-step illustration to calculate the run-up time.

where

Δt = time taken to accelerate during the selected step ΔS in r/min

ΔS = step in r/min

WK^2M = inertia of rotor in the motor in lbs-ft^2 (lbs in mass)

WK^2DE = inertia of mechanical load downstream of the motor in lbs-ft^2

T_a = average accelerating torque in lbsf·ft during the step ΔS in r/min

Recall 1.0 lbs-ft^2 = 1.0 kg-m^2/42.1 × 10^{-3} and 1.0 lbsf·ft = 0.738 N·m

For this example

Recall 1 p.u. or 100% FLT = 31,116 N·m (22,964 lbsf·ft)

$WK^2M + WK^2DE$ = 8314 lbs-ft^2

ΔS = 45 r/min

T_a = 9200 lbsf·ft for the first step of ΔS = 45 r/min

Therefore $\Delta t_1 = \{8314/(308 \times 9200)\}45 = 0.13$ seconds

which is exactly the same as when calculated using metric units. This is repeated for the remaining 19 steps and Table 1.2 gives the results. A simpler method of arriving at all the values of Δt for both 100% and 80% volts is suggested.

First calculate Δt_1 (or any other Δt) by the method previously used to calculate $\Delta t_1 = 0.13$ seconds.

TABLE 1.2 100% Volts, Time Δt in Seconds for Each Step in d_{wr}

Δt_1	Δt_2	Δt_3	Δt_4	Δt_5	Δt_6	Δt_7	Δt_8	Δt_9	Δt_{10}
0.132	0.12	0.12	0.11	0.12	0.12	0.12	0.12	0.12	0.14
Δt_{11}	Δt_{12}	Δt_{13}	Δt_{14}	Δt_{15}	Δt_{16}	Δt_{17}	Δt_{18}	Δt_{19}	Δt_{20}
0.132	0.14	0.15	0.154	0.16	0.17	0.18	0.15	0.1	0.084

But Δt is inversely proportional to the length of the line representing average accelerating torque, so if Δt_1 is calculated via length 1 then Δt_2 must equal Δt_1. *length* 1*/length* 2.

$$\text{That is, } \Delta t_x = \Delta t_1 . l_1 / l_x$$

The summation of all the times for each step gives an estimate of the run-up time $t = 2.6$ seconds. Which is the same as the OEM's data sheet stated a run-up time of 2.6 seconds on a 100% volts supply. This example provides industrial engineers with

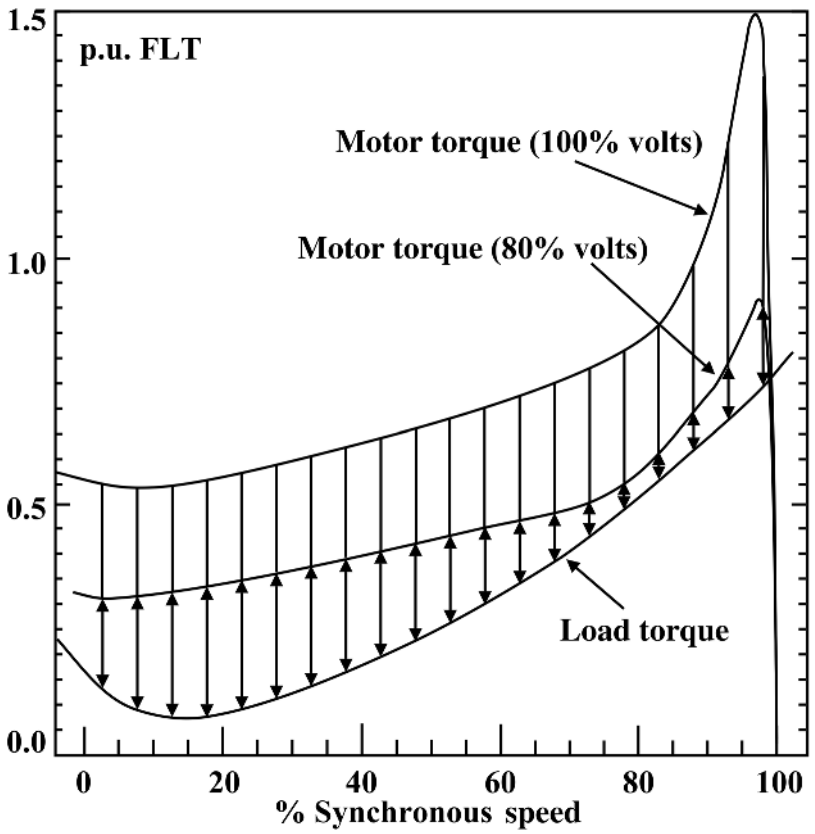

Figure 1.18 Motor torque (100% volts), motor torque (80% volts), and load torque versus synchronous speed—step-by-step calculation of run-up times at different applied volts.

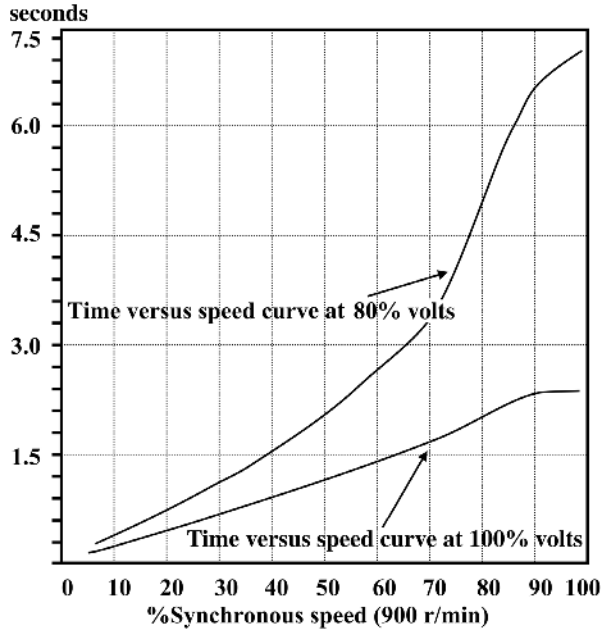

Figure 1.19 Run-up time versus speed for 100% and 80 % volts driving a reciprocating compressor.

knowledge so that they can repeat these calculations, if required to do so, provided they have the torque–speed curves of the motor and load and the total moment of inertia, which should all be available from the OEMs. The client estimated that the voltage would only drop to 95% of its rated value.

As an illustration the torque–speed curve from the motor at 80% volts is shown in Figure 1.18, which shows there is a large drop in the accelerating torque available between 75% and 95 % of the synchronous speed, in visual terms it is "*very thin*" and as Richard Nailen [1.51] very aptly put it in his paper, the available accelerating torque between the load and motor torque–speed curves should be "*as thick as possible.*"

The curves for the run-up time in seconds versus speed for a start up at 100% and 80% volts, respectively, when driving the reciprocating compressor, are shown in Figure 1.19. The results from the step-by-step solution for an applied 80% of

TABLE 1.3 80% Volts, Time Δt in Seconds for Each Step in d_{wr}

Δt_1	Δt_2	Δt_3	Δt_4	Δt_5	Δt_6	Δt_7	Δt_8	Δt_9	Δt_{10}
0.25	0.2	0.18	0.18	0.18	0.18	0.2	0.2	0.25	0.26
Δt_{11}	Δt_{12}	Δt_{13}	Δt_{14}	Δt_{15}	Δt_{16}	Δt_{17}	Δt_{18}	Δt_{19}	Δt_{20}
0.28	0.3	0.37	0.43	0.76	0.95	0.96	0.64	0.38	0.28

rated voltage are given in Table 1.3 and overall the result is that the run-up time has increased to approximately 7.5 seconds, an increase by a factor of 2.9. If this drop in volts were to actually occur, the motor would still start but the rotor bars would be exposed to the starting current for a longer time and thus the thermal stresses, electromagnetic forces, mechanical forces, and bending stresses on the rotor bars and end rings external to the rotor core ends would be present for an undesirable length of time.

An in-depth case history on a completely different HV motor driving a centrifugal pump is presented in Section 6.1 of Chapter 6, in which the cage rotor had 10 broken rotor bars. The cause of the breakages was starting the motor against an open valve pump setting, when it should always have been a closed valve setting. This resulted in much longer run-up times and a stall if the volts dropped to 80% of rated value. All the torque–speed curves are presented in that particular case history.

1.4 ILLUSTRATIONS OF CONSTRUCTION OF A LARGE HV SCIM

Before moving on to further chapters and to support their content, the following Figures 1.20 to 1.26 illustrate the constructional features of a large HV squirrel cage induction motor.

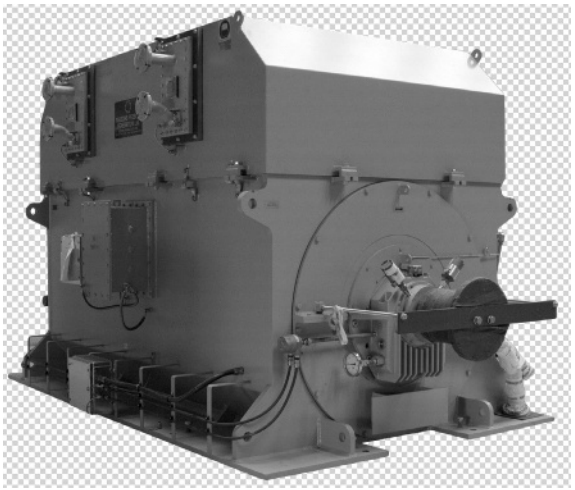

Figure 1.20 3-phase, 13,800 V, 5720 kW/7668 HP, 60 Hz, 1774 r/min SCIM, ready for delivery to the client. Reproduced with permission of Parsons Peebles, Scotland.

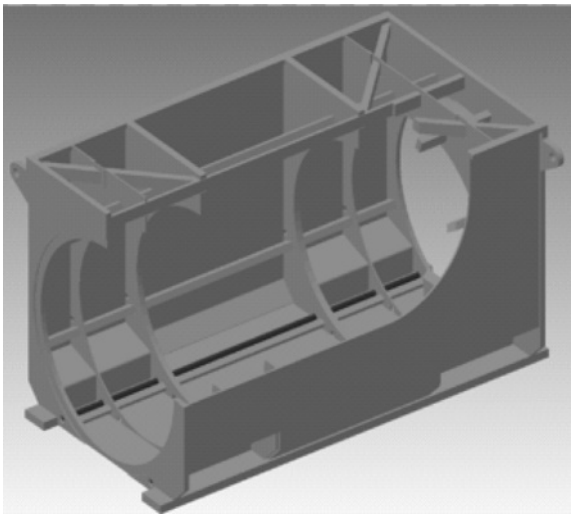

Figure 1.21 Sectional view of frame assembly. Reproduced with permission of Parsons Peebles, Scotland.

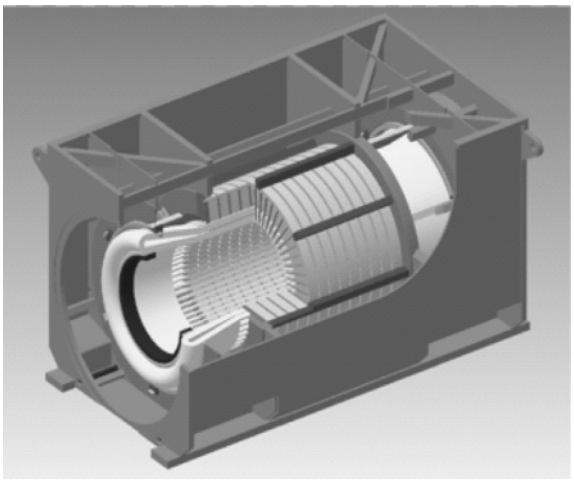

Figure 1.22 Sectional view of frame and stator assembly. Reproduced with permission of Parsons Peebles, Scotland.

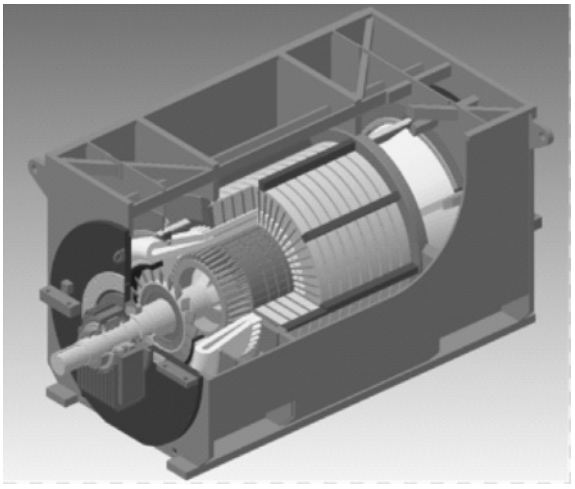

Figure 1.23 Sectional view of frame, stator, and rotor. Reproduced with permission of Parsons Peebles, Scotland.

Figure 1.24 Stator core laminations. Reproduced with permission of Parsons Peebles, Scotland.

Figure 1.25 Squirrel cage rotor. Reproduced with permission of Parsons Peebles, Scotland.

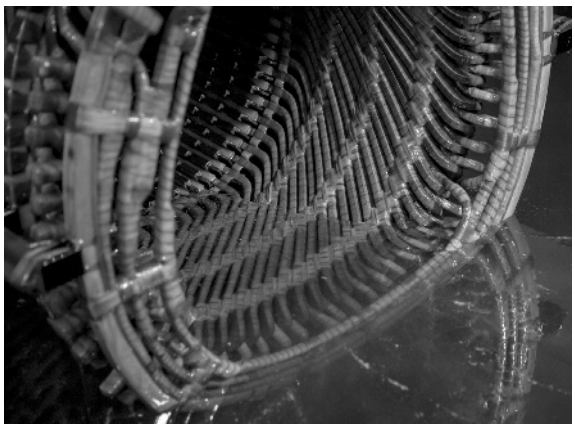

Figure 1.26 HV stator winding and core in process of varnishing. Reproduced with permission of Parsons Peebles, Scotland.

1.5 QUESTIONS

1.5.1 A 3-phase SCIM is connected to a 60 Hz supply and its full-load rated speed is 3580 r/min.

(a) Determine the number of poles.

(b) Calculate the synchronous speed of the rotating magnetic field from the stator winding.

(c) The slip speed in r/min between the stator's rotating field and the actual speed of the rotor is given by $(N_s - N_r)$. Is it correct or incorrect to divide this r/min by 60 and call it the slip frequency with reference to terminology used in induction motor theory? Explain your answer.

(d) Calculate the operating slip in p.u. and as a percentage.

(e) Calculate the slip frequency of the induced emf and current in the rotor conductors.

(f) Repeat (a), (b), (d), and (e) with SCIMs supplied at 60 Hz but when operating at speeds of (i) 1782, (ii) 1185, (iii) 885, and (iv)195 r/min.

(g) A SCIM is fed from a 50 Hz supply and its full-load rated speed is 1470 r/min repeat the calculations for (a), (b), (d), and (e).

1.5.2 The frequency of the currents in the cage winding is constant at all times. Is this statement correct or incorrect? Explain the reasons for your answer.

1.5.3 The speed of the rotating magnetic field produced by the current carrying conductors in the cage winding is at the same speed as the rotor. Is this statement correct or incorrect? Explain the reasons for your answer.

1.5.4 The speed of the rotating magnetic field produced by the current carrying rotor conductors is not at the same speed as the rotating magnetic field produced by the stator winding with respect to a stationary observer on the stator. Is this statement correct or incorrect? Explain the reasons for your answer.

1.5.5 For a 3-phase, star connected, 460 V SCIM, 74.6 kW/100 HP, 60 Hz, 1782 r/min, 0.88 p.f. and an efficiency of 96.5%, calculate the following

(a) The nominal full-load rated current.

(b) The nominal FLT in Nm and in lbsf ft.

1.5.6 For the motor specified in Question 1.5.5, the mechanical load on the motor is reduced and the speed increases to 1792 r/min.

(a) What is the new output power and torque at the shaft in kW and HP and in lbsf ft and in N·m? Hint: Refer to Figures 1.15 and 1.15a and the associated text and worked example.

(b) During another change in the mechanical load on this motor the input current drops to 50% of rated FLC, which means that the motor is delivering 50% of its rated full-load power and torque output. Is this statement correct or incorrect? Justify your answer.

1.5.7 Why does a SCIM take a much larger current during a DOL start compared to its rated FLC?

1.5.8 What are the various undesirable effects on the copper cage winding caused by a DOL start?

1.5.9 Why does a SCIM run-up faster on no-load compared to the time taken when connected to a mechanical load?

1.5.10 For the torque–speed curves of the motor and load shown in Figure 1.17 with the same total inertia determine the run-up time when the supply volts is 90% or 0.9 p.u. of the rated volts.

REFERENCES

[1.1] N. Tesla, "A new system of alternate current motors and transformers," *Transactions of American Institute of Electrical Engineers*, vol. V, no. 10, 1888, pp. 308–327.

[1.2] Source en.wikipedia.org/wiki/electricity consumption.

[1.3] G. C. Stone, E. A. Butler, I. Culbert, and H. Dhiranai, *Electrical Insulation for Rotating Machines – Design, Evaluation, Testing and Repair*, Wiley-IEEE Press, 2004, ISBN 0-471-44506-1.

[1.4] P. Tavner, L. Ran, J. Penman, and H. Sedding, *Condition Monitoring of Rotating Electrical Machines*, IET Power and Energy Series 56, The Institution of Engineering and Technology, London, UK, 2008, ISBN 978-0-86341-739-9.

[1.5] H. A. Toliyat, S. Nandi, S. Choi, and H. Meshgin-Kilk, *Electric Machines-Modeling, Condition Monitoring and Fault Diagnosis*, CRC Press Taylor & Francis Group, New York, 2013, ISBN 978-0-8493-7027-4.

[1.6] W. T. Thomson, *MCSA Industrial Case Studies Proves the On-Line Detection of Airgap Eccentricity in HV Induction Motors*, PCIC Europe, International European Conference, London, June 2015.

[1.7] W. T. Thomson, *MCSA Case Histories on Detection of Broken Rotor Bars in Induction Motors - Including Influences of Mechanical Load Dynamics on the Analysis*, COMET Conference, 2014, Hosted by Iris Power Qualitrol, Canada, in Austin TX, December 2014.

[1.8] W. T. Thomson and M. Fenger, "Case Histories of Current Signature Analysis to Detect Faults in Induction Motor Drives," Proceedings of IEEE International conference on Electrical Machines and Drives (IEMDC), University of Wisconsin, Madison, WI, June 2003.

[1.9] W. T. Thomson and R. J. Gilmore, "Motor Current Signature Analysis to Detect Faults in Induction Motor Drives - Fundamentals, Data Interpretation and Industrial Case Histories," Proceedings of 32nd Turbomachinery Symposium, A&M University, TX, September 2003.

[1.10] W. T. Thomson and P. Orpin, "Current and Vibration Monitoring for Fault Diagnosis and Root Cause Analysis of Induction Motors," Proceedings of 31st Turbomachinery Symposium, A&M University, TX, September 2002.

[1.11] W. T. Thomson and W. H. Ross, "Application of MCSA to a Diverse Range of Induction Motor Drives in Power Stations," Iris Rotating Machines Conference, IRMC 01, Washington, D.C., June 2001.

[1.12] M. Fenger, M. Susnik, and W. T. Thomson, "Development of a Fully Portable Current Signature Analysis Meter to Detect Electrical and Mechanical Faults in Induction Motor Drives," Iris Rotating Machines Conference, IRMC 01, Washington, D.C., June 2001.

[1.13] W. T. Thomson and M. Fenger, "Current signature analysis to detect induction motor faults", *IEEE Industry Applications Magazine*, vol. 7, no. 4, 2001, pp. 26–34.

[1.14] W. T. Thomson, D. Rankin, and D. G. Dorrell, "On-line current monitoring to diagnose airgap eccentricity in large 3-phase induction motors - an industrial case history verifies the predictions", *IEEE Transactions on Energy Conversion*, vol. 14, no. 4, December, 1999, pp. 1372–1378.

[1.15] W. T. Thomson and A. Barbour, "The On-Line Prediction of Airgap Eccentricity Levels in Large (MW Range) 3-Phase Induction Motors," Proceedings of IEEE, IEMDC Conference, Seattle, WA, May 1999—US$1000 best paper award.

[1.16] W. T. Thomson and A. Barbour, "An Industrial Case Study of On-Line Current Monitoring and Finite Element Analysis to Diagnose Airgap Eccentricity Problems in Large High Voltage 3-phase

Induction Motors," Proceedings of the 9th IEE International Conference on Electrical Machines and Drives (EMD), Canterbury Christ Church College, UK, September 1999.

[1.17] W. T. Thomson, "A Review of On-Line Condition Monitoring Techniques for Three-Phase Squirrel-Cage Induction Motors -Past Present and Future," Keynote address at IEEE Symposium on Diagnostics for Electrical Machines, Power Electronics and Drives, Gijon, Spain, September 1999 pp. 3–18.

[1.18] W. T. Thomson and A. Barbour, "On-line current monitoring and application of a finite element method to predict the level of airgap eccentricity in 3-Phase induction motors", *IEEE Transactions on Energy Conversion*, vol. 13, no. 4, December 1998, pp. 347–357 (includes discussion and closure).

[1.19] W. T. Thomson, A. Barbour, C. Tassoni, and F. Filippetti, "An Appraisal of the MMF-Permeance Method and Finite Element Models to Study Static Airgap Eccentricity and its Diagnosis in Induction Machines," Proceedings of ICEM'98, Istanbul, 1998.

[1.20] W. T Thomson, D. Rankin, and D. G. Dorrell, "On-line Current Monitoring to Diagnose Airgap Eccentricity - An Industrial Case History of Large HV, 3-Phase Induction Motors," Proceedings of IEEE International, Conference, IEMDC'97, Milwaukee, WI, May 1997.

[1.21] D. G. Dorrell, W. T. Thomson, and S. Roach, "Analysis of airgap flux, current and vibration signals as a function of the combination of static and dynamic airgap eccentricity in 3-Phase induction motors", *IEEE Transactions on Industry Applications*, vol. 33, no. 1, January/February 1997, pp. 24–34.

[1.22] A. Barbour and W. T. Thomson, "Finite Element Study of Rotor Slot Designs with respect to Current Monitoring for detecting Static Airgap Eccentricity in Squirrel-cage Induction Motors," Proceedings of IEEE Industrial Applications Conference, New Orleans, LA, October 1997.

[1.23] A. Barbour and W. T. Thomson, "Finite Element Analysis and On-Line Current Monitoring to Diagnose Airgap Eccentricity in 3-Phase Induction Motors," Proceedings of IEE International Conference, EMD, University of Cambridge, September 1997.

[1.24] D. G. Dorrell, W. T. Thomson, and S. Roach, "Combined Effects of Static and Dynamic Eccentricity on Airgap Flux Waves and the Application of Current Monitoring to Detect Dynamic Eccentricity in Three-phase Induction Motors," IEE International Conference on Electrical Machines and Drives, September 1995.

[1.25] D. G. Dorrell, W. T. Thomson, and S. Roach, "Analysis of Airgap Flux, Current and Vibration Signals as a Function of the Combination of Static and Dynamic Airgap Eccentricity in Three-phase Induction Motors," IEEE International Conference on Industry Applications, Orlando, FL, October 1995.

[1.26] W. T. Thomson, "On-Line Current Monitoring - The Influence of Mechanical Loads/Unique Rotor Designs on the Detection of Broken Rotor Bars in Squirrel Cage Induction Motors," ICEM '92, UMIST, September 1992.

[1.27] S. Elder, J. F. Watson, and W. T. Thomson, "The Analysis of Transient Currents in Induction Motors for the Purpose of Detecting Rotor Faults," Proceedings of the 25th Universities Power Engineering Conference, RGIT, Aberdeen, September 1990.

[1.28] W. T. Thomson, J. R. Cameron, and A. B. Dow, "On-Line Diagnostics of Large Induction Motors," NATO ARW (by invitation only), Catholic University of Leuven, Belgium, August 1986, published in the NATO Api Series, Pub Martines Hijhoff, July 1988.

[1.29] W. T. Thomson and I. D. Stewart, "On-Line Current Monitoring for Fault Diagnosis in Inverter Fed Induction Motors," Proceedings of IEE 3rd International Conference in Power Electronics and Variable Speed Drives, Savoy Place, London, July 1988.

[1.30] W. T. Thomson, J. R. Cameron, and A. B. Dow, "On-Line Current Monitoring and Analysis to Quantify the Level of Airgap Eccentricity in Induction Motors," Proceedings of International Conference in Electrical Machines, ICEM '88, Pisa, Italy, September 1988.

[1.31] J. R. Cameron, W. T. Thomson, and A. B. Dow, "On-Line Current Monitoring of Induction Motors - A Method of Calculating The Level of Airgap Eccentricity," Proceedings of IEE EMDA '87 Conference, London, November 1987.

[1.32] W. T. Thomson and D. Rankin, "Case Histories of Rotor Winding Fault Diagnosis in Induction Motors," Proceedings 2nd International Conference on Condition Monitoring, University College of Swansea, March 1987.

[1.33] W. T. Thomson, S. J. Chalmers, and D. Rankin, "On Line Current Monitoring and Fault Diagnosis in HV Induction Motors - Case Histories and Cost Savings in Offshore Installations," SPE Proceedings of Offshore Europe '87 Conference, Aberdeen, September, 1987.

[1.34] J. R. Cameron, W. T. Thomson, and A. B. Dow, "Vibration and current monitoring for detecting airgap eccentricity in large induction motors", *IEE Proceedings*, vol. 133, Part B. no 3, May 1986.

[1.35] J. R. Cameron, W. T. Thomson, and A. B. Dow, "A New On-Line Current and Vibration Monitoring Technique for Detecting Airgap Eccentricity in Large Induction Motors," Proceedings of IEE EMDA '85 Conference, Savoy Place, London, November 1985.

[1.36] W. T. Thomson, N.D. Deans, R. A. Leonard, and A. J. Milne, "Monitoring Strategy for Discriminating Between Different Types of Rotor Cage Faults," Proceedings 18th Universities Power Engineering Conference Proceedings, University of Surrey, Surrey, April, 1983.

[1.37] I. Culbert, H. Jivajee, and P. Laderoute, "Case Studies with New Current Signature Analysis Technology," IRIS Rotating Machines Conference, New Orleans, LA, June 14–17, 2004

[1.38] I. Culbert and H. Jivajee, "New Current Signature Analysis Technology to Reliably Detect Cage Winding Defects and Abnormal Airgap Eccentricity in Induction Motors," EXFOR 2005, Palais des Congress, Montreal, QC, Canada, February 8–10, 2005.

[1.39] M. Fenger, I. Culbert, and B. Lloyd, "Case Histories of Current Signature Analysis to Detect Faults in Induction Motor Drives," IEEE-IAS/PCA Cement Industry Conference, Dallas, TX, May 4–9, 2003.

[1.40] I. M. Culbert, and W. Rhodes, "Using current signature analysis technology to reliably detect cage winding defects in squirrel-cage induction motors", *IEEE-TIA*, vol. 43, no. 2, March/April 2007.

[1.41] I. Culbert, "Motor Maintenance Testing & Diagnostics On-Line, Off-Line," IEEE 55th Annual IEEE Pulp and Paper Conference, Renaissance Ross Bridge Golf Resort & Spa, Birmingham, AL, June 21–26, 2009.

[1.42] G. C. Stone, M. Sasic, D. Dunn, and I. Culbert, "Recent Problems Experienced with Motor and Generator Windings," IEEE PCIC 2009, Anaheim, CA, September 14–16, 2009.

[1.43] G. B. Kliman and J. Stein, *Methods of Motor Current Signature Analysis Electric Machines and Power Systems*, Hemisphere Publishing, New York vol. 20, 1982.

[1.44] G. B. Kliman, R. A. Koegl, J. Stein, R. D. Endicott, and M. W. Madden, "Non-invasive detection of broken rotor bars in operating induction motors", *IEEE Transactions on Energy Conversion*, vol. 3, no. 4, December 1988, pp. 873–879.

[1.45] S. Williamson, and S. C. Smith, "Steady-state analysis of 3-phase cage motors with rotor-bar and end-ring faults", *IEEE Proceedings B-Electric Power Applications*, vol. 129, no. 3, 1982.

[1.46] P. Vas, "Steady state and transient performance of induction motors with rotor asymmetry", *IEEE Transactions on Power Apparatus band Systems*, vol. PAS-101, no. 9, September 1982, pp. 3246–3251.

[1.47] W. Deleroi, "Broken Bar in Squirrel-Cage Rotor of an Induction Motor," Part I, Description by Superimposed Fault Currents, Archiv fur Eleektrotechnik 67, 1984, pp. 91–99

[1.48] C. Hargis, B. Gaydon, and K. Kamish, "The Detection of Rotor Defects in Induction Motors," Proceedings of 1st IEE International Conference on Electrical Machines, Design and Application. London, UK, pp. 216–220.

[1.49] P. Tavner, K. E. Armin, and C. Hargis, "An Electrical Technique for Monitoring Induction Cage Rotors", Proceedings of 3rd IEEE International Conference on Electrical Machines and Drives, London, UK, pp. 43–46.

[1.50] F. Filippetti, G. Franceschini, M. Martelli, and C. Tassoni, "An Approach to a Knowledge Representation about Induction Machine Diagnostics in Expert Systems," International Conference on Electrical Machines ICEM'88, Pisa, Italy, September 1988.

[1.51] R. L. Nailen, "Large motor starting problems in the petroleum industry", *IEEE Transactions on Industry and General Applications*, vol. IGA-5, no. 4, 1969, pp. 422–427.

[1.52] R. L. Nailen, "New rotor design concept solves pipeline motor acceleration" *IEEE Transactions on Industry Applications Problem*, vol. IA-9, no. 2, 1973, pp. 201–205.

[1.53] M. E. H. Benbouzid, "Bibliography on induction motors faults detection and diagnosis" *IEEE Transactions on Energy Conversion*, vol. 14, no. 4, December 1999, pp. 1065–1074.

[1.54] M. E. El-Hawary, *Principles of Electric Machines with Power Electronic Applications*, 2nd edition, Hardcover, Wiley-IEEE Press, July 2002.

[1.55] M. Liwschitz-Garik and C. C Whipple, *Electric Machinery Vol. II, A-C Machines,* Van Nostrand Company, 1st published, September 1946.
[1.56] M. G. Say, *Alternating Current Machines*, 4th edition, ELBS and Pitman Publishing, 1976.
[1.57] P. C. Sen, *Principle of Electrical Machines and Power Electronics*, 2nd edition, John Wiley & Sons, 1997.
[1.58] A. Chapman, *Electric Machinery Fundamentals*, McGraw Hill, 1985.
[1.59] A. Hughes, *Electric Motor and Drives – Fundamentals, Types and Applications*, Butterworth-Heinemann, 1990.
[1.60] G. Slemon, *Electric Machines and Drives*, Addison-Wesley Publishing Company Inc., 1992.
[1.61] P. L. Alger, *Induction Machines-Their Behavior and Uses*, Gordon and Breach Science Publications Inc., 2nd edition, published by OPA Amsterdam, 3rd printing with additions, 1995.
[1.62] H. Vickers, *The Induction Motor*, Sir Isaac Pitman and Sons Ltd., London (1st edition, 1924; 2nd edition 1953).
[1.63] M. M. Liwschitz-Garik, Computation of skin effect in bars of squirrel-cage rotors [includes discussion, *Power Apparatus and Systems, Part III. Transactions of the American Institute of Electrical Engineers*, vol. 74, no. 3, 1955.
[1.64] J. H. Dymond, Stall time, acceleration time, frequency of starting: the myths and the facts [electric motors], *IEEE Transactions on Industry Applications*, vol. 29, no. 1, 1993, pp. 42–51.
[1.65] P. Dunsheath, *A History of Electrical Engineering*, Faber and Faber, 1st published in 1962.
[1.66] NEMA MG1: "Motors and Generators," 2012.